

Film-substrate hydrodynamic interaction initiated by femtosecond laser irradiation

V. A. Khokhlov, N. A. Inogamov, V. V. Zhakhovsky, D. K. Ilitsky, K. P. Migdal, and V. V. Shepelev

Citation: **1793**, 100038 (2017); doi: 10.1063/1.4971663

View online: <http://dx.doi.org/10.1063/1.4971663>

View Table of Contents: <http://aip.scitation.org/toc/apc/1793/1>

Published by the [American Institute of Physics](#)

Film-substrate hydrodynamic interaction initiated by femtosecond laser irradiation

V.A. Khokhlov^{1,a)}, N.A. Inogamov^{1,2,b)}, V.V. Zhakhovsky^{2,c)}, D.K. Ilnitsky²,
K.P. Migdal² and V.V. Shepelev³

¹*Landau Institute for Theoretical Physics of the Russian Academy of Sciences,
Akademika Semenova 1a, Chernogolovka 142432, Russia*

²*Dukhov Research Institute of Automatics (VNIIA), Sushchevskaya 22, Moscow 127055, Russia*

³*Institute for Computer-Aided Design of the Russian Academy of Sciences,
Vtoraya Brestskaya 19/18, Moscow 123056, Russia*

^{a)}Corresponding author: khokhlov@landau.ac.ru

^{b)}nailinogamov@gmail.com

^{c)}6as1z@gmail.com

Abstract. Action of an ultrashort single laser pulse onto a thin metal film is considered. Disruption of a plane freestanding film quickly heated by a laser is the simplest model of the laser thermomechanical spallation. There is a sharp spallation (ablation) threshold F_{abl} dividing dynamics of a freestanding film to two regimes: below or above the threshold F_{abl} . Problem of significant importance is: how this picture will change when a film is deposited onto a substrate? We have solved this problem. It is found that there are two thresholds $F_{delam} < F < F_{abl}$ and the four regimes of motion relative to the case of a freestanding film. For the range of fluences $0 < F < F_{delam}$ a film oscillates remaining on a substrate. Oscillations decay in time due to irradiation of the sonic waves into substrate. For $F_{delam} < F < F_{abl} + \Delta F$ the film delaminates from the substrate because negative pressure (tensile stress) propagating from the vacuum boundary with the rarefaction acoustic wave achieves the film-substrate contact boundary and overcomes adhesion strength of a contact. The addition ΔF to the freestanding case is small in the case when the ratio η of the acoustic impedances of substrate to a film is small. This is the case of the gold or silver films on a glass. The third is the complicated regime with interacting delamination and spallation processes when $F \approx F_{abl} + \Delta F$. In the fourth regime $F_{abl} + \Delta F < F$ there is the disruption of a film into two halves. The external half flies away while the internal one remains on substrate.

1. Screening of Light in Metals: Competition between Skin Depth and Heat Affected Zone

Laser ablation by the ultrashort pulses is used in many applications; e.g., laser induced forward transfer, nanophotonics [1, 2], an interference fabrication of nanohole arrays [3, 4], nanoparticles fabrication [5], and others. In the paper an action of an optical laser onto metals is considered. Optical electromagnetic wave is absorbed in a nanothin $\delta_{skn} = \lambda/2/(2\pi)/k \approx 10 \div 20$ nm skin layer; here $k \sim \omega_{pl}/\omega$ is an extinction coefficient, ω_{pl} is plasma frequency, ω is frequency of an electromagnetic wave. Absorption is described in the approximation of electrodynamics of continuous media (electron free path is supposed to be less than δ_{skn}). In the case of metals the plasma frequency is high, thus a significant factor appears which strongly decreases the skin depth. Indeed, the extinction coefficient k is large, and skin is thin relative to the wavelength $\lambda \sim 1 \mu\text{m}$. We use two-temperature hydrodynamic modeling of motion beginning with this extra small spatial scale δ_{skn} . Hydrodynamic description is valid if absorbed energy F_{abs} is higher than a few mJ/cm². Because the electron-electron relaxation lasts less than 100 fs in this energy range and the ion-ion relaxation takes a few phonon oscillations; typical phonon period is $\sim 100 \div 200$ fs $\sim 1/10$ THz. While a sonic wave runs a skin during a few picoseconds (ps). Creation of a heat affected layer d_T by a supersonic two-temperature electronic thermal wave also takes a few ps. In the bulk metal targets the thickness d_T is equal to $5 \div 7$ thicknesses δ_{skn} . Below we consider the gold films $50 \div 100$ nm thick. We can describe light absorption and heat propagation using the diffusion approximation because an electron mean free path for our electron temperatures is of the order of several interatomic distances. Simulations were done for gold and silver films, but general results concerning the delamination and ablation thresholds mentioned in Abstract are valid for semiconductors and other metals also.

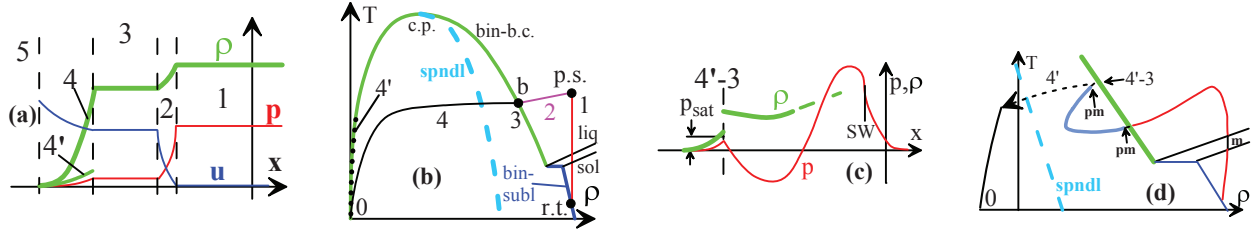


FIGURE 1. (a) The self-similar profiles consisting of 1-2-3-4-5 regions correspond to the rarefaction wave propagating into the homogeneous pressurized condensed half-space region indicated by 1. Region 2 describes expansion of condensed matter. Homogeneous flow in 3 corresponds to the intersection point of an isentropic curve and a binodal. The tail 4 presents material inside the region encircled by the binodal curve. The point between the 1 and 2 runs with sound speed into region 1. The profiles u, p, ρ present the distributions of velocity, pressure, and density. Figure (b) shows thermodynamic conditions along the self-similar rarefaction of condensed substance. The curve binodal "bin" divides one- and two-phase regions in the equilibrium case and separates stable $p = p_{sat}$ and metastable $p < p_{sat}$ states in the non-equilibrium case, here $p_{sat}(T)$ is pressure of saturated vapor. The parts of the binodal curve are: the sublimation curve "bin-subl" and the boiling curve "bin-b.c.". The triple point is between them. (c) Transformation of the self-similar flow shown in (a) for the non-self-similar case. Pressure profile with a finite heating depth d_T generates the typical z-type wave profile of hill $p > 0$ and well $p < 0$. In the self-similar case the depth is $d_T = \infty$. The tail 4' and the jump 4'-3 remains approximately the same as in (a). But now the pressure p_3 in the point 3 is of the order of the saturation pressure $p_3 < p_{sat}$ (not $p_3 = p_{sat}$). In the bulk target the z-profile runs to the right leaving the surface layer growing in thickness with material in the near binodal states. Overturning of the compression hill after some traveling distance produces a shock "SW". (d) The z-profile at the phase map resembles the instant spatial profile shown in Fig. (c). With time the whole z-profile moves down, passing the melting zone ("m"), and coming closer and closer to the room temperature point. Material in the surface layer, which is behind the moving down blue well of $p < 0$, remains near the state 4'-3 at the binodal (because cooling is slow). The pressures at the binodal curve are positive. All condensed matter below the binodal is in the metastable states. The arrows "pm" (plus/minus) indicate points where the pressure becomes negative.

2. Supersonic Expansion of Heat from a Skin Layer while Electrons are Hot and Decoupled

Laser action causes significant hydrodynamic phenomena in our range of absorbed fluences $F_{abs} \sim 10 \div 100 \text{ mJ/cm}^2$ and pulse durations $\tau_L \sim 0.1 \div 1 \text{ ps}$. It is important that the temporal duration t_T of the supersonic creation a heat affected layer d_T or heating of a whole metal film through (in the cases when a thickness d_f of a film is less than d_T) is less than the duration of the pressure dynamical (i.e., due to volume expansion) relaxation of a heat affected zone d_T or d_f . This is a result of *supersonic* spreading of heat absorbed in a skin layer out of this layer at the time of the two-temperature stage. At the two-temperature stage, the heat spreads along the electron subsystem partially decoupled from the thermally capacacious ion subsystem. As was said, pressure relaxes during the longer sonic time scale $t_s = d_T/c_s$ or d_f/c_s than the duration t_{eq} of the electron-ion temperature equilibration. Thus the laser action transfers a thin film $d_f < d_T$ almost instantaneously (for the subsequent hydrodynamic motion) into approximately homogeneously heated (heated and hence pressurized) state. The instantaneity of heating is used below only for qualitative estimates, simulations of course don't use this approximation. For the bulk targets the ratio t_s/t_{eq} is $\sim 10 \div 20$ for such metals as Al, Ni, Fe, Pt, and others with a rather large coupling parameter. Even in the case of gold when an electron-ion exchange is not fast, this parameter is $3 \div 4$. The first part of a bulk target is expanded during the two-temperature stage under influence of electron pressure. Thickness of this part is $\approx (t_{eq}/t_s)d_T$.

Mass expansion time t_s is small $t_s < t_{eq}$ in the case of the ultrathin films $d_f \leq \delta_{skn}$. Then expansion is driven mainly by electron pressure. Below we will consider a gold and silver films with $d_f \sim 50 \text{ nm} \approx (2 \div 3)\delta_{skn} \approx d_T/(2 \div 3)$. Those films are used in the applications [1, 2, 3, 4, 5, 6, 7]. For them an alignment of electron temperature T_e along a film thickness takes $t_T \sim 1 \text{ ps}$, while an acoustic time scale $t_s = d_f/c_s \sim 20 \text{ ps}$ is of the order of duration of a two-temperature stage $t_{eq} \sim 5 \div 10 \text{ ps}$ for gold. In this case an acceleration of a vacuum boundary driven initially by electron pressure gradually increases thanks to transfer from the electron driver to the ion driver. At the end of a two-temperature relaxation the pressure of ion subsystem p_i is higher than initial (after a pulse) electron pressure p_e at the same density and the same energy per unit of volume because the ion Gruneisen parameter is higher than the electron Gruneisen parameter. Therefore the maximum total pressure $p = p_e + p_i$ increases during the two-temperature stage. We see that the energy transit from electrons to ions causes additional acceleration. This circumstance significantly changes the rarefaction profiles considered below. As a result of those changes, the rarefaction profile differs from the profile for the decay of the homogeneous distribution, although for $t_T < t$ the distribution of electron temperature T_e

is almost homogeneous. The leveling of T_e means that the heat conduction becomes insignificant, and matter expands in the approximately adiabatic regime. But this is the combined electron-ion adiabatic expansion pumping an electron entropy into an ion entropy during the two-temperature part of rarefaction.

If the heated layer d_T in a bulk target is sufficiently hot to cause fast melting than people say about the homogeneous melting of the layer $\sim d_T$. This regime of melting cannot be described in the Stefan problem approximation with a thin melting front separating pure solid and liquid. People oppose the homogeneous melting to the heterogeneous melting. The homogeneous melting is supersonic one since $d_T/c_s > t_{eq}$. Supersonic propagation of heat is possible because the Fermi velocities of electrons are $\sim \sqrt{M/m}$ times larger than speed of sound [8, 9], here M and m are ion and electron masses. In the supersonic case the fused layer d_T passes the sequence of the two-phase liquid-solid mixed states with increasing liquid content during the time interval $t_{eq} \sim t_T$ or faster and turns into pure liquid [8, 9, 10, 11]. Fast melting, lasting few phonon oscillations, takes place when a solid is overheated above the spinodal of melting. The melting spinodal locates $\sim 20 - 40\%$ above a melting curve.

3. Single Expansion Wave: Difference Between Dynamics of Condensed and Gaseous Media

Hydrodynamic decay into vacuum of the homogeneous pressurized half-space filled with condensed matter was studied in [12, 13, 14, 15, 16]. For the first time, the nontrivial thermodynamic equation of state was used to describe hydrodynamics of ablation in paper [12]. The hydrodynamic expansion of a *condensed* state results in a rather specific (qualitatively different from a rarefaction in the case of *gaseous* matter) rarefaction wave which unloads pressurized substance "p.s." from the point 1 in Figs. 1 (a,b) into the point 3 "b" in those Figures. The peculiarity with the binodal appears as a result of cohesive interaction in condensed matter versus the pure repulsion in gas. Therefore pressure of condensed substance drops to zero $p = 0$ after a small volume expansion; compare with a huge expansion necessary for gas to achieve $p = 0$. The point 3 ("b") is at the binodal curve "bin" in the phase diagram of an irradiated substance shown in Fig. 1(b). Position of this point depends on absorbed energy F_{abs} : if energy is higher - then the point 3 "b" at the binodal moves along the binodal more close to the critical point "c.p." in Fig. 1(b). Energy F_{abs} defines entropy s corresponding to the approximately isentropic profiles u, ρ, p 1-2-3-4-5 in Fig. 1(a) and to the curve 1-2-3-4-0 in Fig. 1(b). Usually the slope of the isentropic curve in the condensed phase is less than the slope of the melting curves solidus "sol" and liquidus "liq" in Fig. 1(b). Therefore solid may melt along an unloading isentropic curve if this particular curves starts in the solid state near the solidus "sol"; see paper [17] and Fig. 1 in paper [18].

Existence of the point 3 "b" in Fig. 1(b) means that it is possible to keep finite density ρ_{3b} of a condensed substance at small (almost zero outside a critical point "c.p.") pressures equal to saturated vapor pressure. For moderate values F_{abs} corresponding to the near ablation threshold values, the density ρ_{3b} is more than 50% of the solid state density. Mass concentrated in the point 3 "b" in Fig. 1(b) is *finite* for the self-similar rarefaction wave 1-2-3-4-5 shown in Fig. 1(a). Thus the finite amount of mass is accumulated in the thermodynamical point. This means that all particles forming this mass have equal thermodynamic parameters. The point 3 "b" in Fig. 1(b) corresponds to the piece 3 of a homogeneous flow in Fig. 1(a). The ratio of masses m_3/m_4 of the pieces 3 and 4 at the profile 1-2-3-4-5 in Fig. 1(a) is exponentially large at small temperatures and decreases as the value F_{abs} increases. The homogeneous piece 3 disappears near the critical point.

The pieces 1, 2, and 3 of the rarefaction wave in Fig. 1(a) are easily described by a linear acoustics. Linear approximation is valid if pressure p_1 in the state 1 in Fig. 1(b) is small: $p_1 \ll K$, here K is a bulk module. Usually pressure $p_1 \sim 0.3K$ at the ablation threshold for thin films [19]. Integrating the linear equations $\rho_t + \rho u_x = 0$, $\rho u_t + p_x = 0$ we obtain that the density drop $\Delta\rho = \rho_1 - \rho_3$ among the points 1 and 3 is $\Delta\rho = (p_1/K)\rho$ and the mass accumulated in the point 3 "b" moves to the vacuum side with velocity $= p_1/z$, where $z = \rho c$ is acoustic impedance. In the bulk targets for long propagations the acoustic dispersion is significant if the values of p_1/K are not small, see Fig. 4. in [20].

4. Gaseous piece of expansion profile: stable vapor-liquid mixture versus evaporation

The highest vapor pressure is limited by a critical pressure $\sim 0.4 - 0.8$ GPa, whereas pressures in the pressurized layer 1 in Figs. 1(a,b) are $p_1 \sim 5$ GPa and larger in our conditions. Therefore above it is said "small" relative to the vapor pressure. It is small and thus is dynamically insignificant in comparison with pressures in the condensed matter driving accelerations and expansion. In the gas case the rarefaction profile is 1-2-0, that is the pieces 3 and 4 are absent in gas together with binodal and two-phase region. The piece 4 (Figs. 1 a,b) of the self-similar hydrodynamic expansion in the condensed phase case passes through the two phase region in the ρ, T plane of the phase diagram in Fig. 1(b). Thus the rarefaction wave is a sum of the three pieces: the piece 2 from the pressurized state "p.s." to the binodal "b,"

the piece 3 presenting the finite and growing in time mass at the binodal (localized in the point 3 "b"), and the piece 4 corresponding to the two-phase tail 4 [13, 14]. It is necessary to emphasize that the content of the tail 4 depends on the model. There are different hydrodynamic descriptions, different equation of states (EoS), molecular dynamics, and reality. Let us discuss them. The tail 4 in Fig. 1(b) corresponds to the equilibrium EoS. In this case the binodal separates the stable one-phase region above the binodal and the *stable two-phase* region below the binodal. The tail 4 continuously connect the point 3 and vacuum $\rho = 0, p = 0$. This is an adiabatic expansion, therefore temperature drops down and the point $\rho = 0, T = 0$ is achieved.

The rarefaction flow starting from a condensed state at finite temperature, e.g., from the point 1 in Fig. 1(b), cannot finish in the point 3 at the binodal, because the vacuum boundary condition demands $p = 0$, while the pressure in the point 3 is $p_{3b} = p_{sat} > 0$, where p_{sat} is a saturated vapor pressure at the temperature corresponding to the point 3 "b". We have to fill up the gap between the p_{sat} and $p = 0$. If we use the stable two-phase EoS for the vapor phase and the "follow-through" hydrodynamic code for description of the transonic rarefaction then we inevitably come to the two-phase tail filling the gap; here the "follow-through" means that the condensed and the vapor phases are not separated by the evaporation/condensation front conditions. This conclusion is true for the Lagrangian [21] and Euler hydrodynamics [22]. There are another approaches which use the extraction of the evaporation front [23, 24, 25]. In our approach we use the hydrodynamic code [21] *together* with the molecular dynamics (MD) code. This gives us significant advantages because those codes complete each other as may be understood from Fig. 7 in [8] where the ultrafast melting processes simulated by both codes are compared.

MD simulations reveal that for our very small spatiotemporal scales the transfer of the overcooled vapor into the equilibrium two-phase mixture through nucleation of the valuable droplets is significantly delayed. The dashed curve 4' in Fig. 1(b) corresponds to the gaseous tail according to MD. The curve 4' begins with the point corresponding to vapor with temperature of the order of temperature in the point 3 "b" in Fig. 1(b) and density of the order of density of saturated vapor for this temperature. The starting point of the curve 4' is in geometrical contact with the point 3 "b", see Fig. 1(a). Density of the curve 4' jumps down at the boundary 4-3 in Fig. 1(a). The curve 4' continues down to the vacuum $\rho = 0, T = 0$ in Fig. 1(b). The curve 4' locates somewhere in the two-phase region near the left branch of the binodal called the condensation curve. If we increase fluence F_{abs} then the temperatures of the starting point of the curve 4' and the point 3 increase, the points become higher in the ρ, T phase map and more close to each other. Of course, the dependencies 4 and 4' are qualitatively and quantitatively different. Qualitatively the tail 4 is a vapor-liquid mixture, while the 4' is vapor. Total mass of the tail 4' is less. Density at the profile 4 in Fig. 1(a) sharply decreases as we deviate from the boundary 4-3 because sound velocity in the equilibrium vapor-liquid mixture is very low [13, 14]. Sound velocity in a mixture defines a density gradient. Therefore the sharp density decrease in the tail 4 mimic the jump in the tail 4'. The differences among the tails 4 and 4' are of small importance for dynamics of the dense pieces 2 and 3 in Fig. 1(a,b) in the case of the moderate fluences F_{abs} when temperature in the point 3 is less than 50% of the critical temperature. For the case of a film delaminated from a substrate namely this case is important.

We describe above the situation with a single rarefaction wave running the *homogeneous* half-space because this is the basic element for understanding of the film laser delamination process where the interplay of expansions separates a film [18]. Now we are ready to consider the *inhomogeneous* case. But before let us conclude with the analysis of the qualitative differences between the tail 4' and the dense pieces 3 and 2 moving to the vacuum side, see velocity profile in Fig. 1(a). As was said, in reality there are the density jump at the boundary 4'-3 and a pure vapor content of the tail 4'. This follows from MD. In the homogeneous case the content of the pieces 3 and 2 is continuous condensed matter. In the inhomogeneous case and above the ablation threshold F_{abl} the tail 4' remains purely gaseous but the new two important details appear in the range of fluences $F_{abl} < F < F_{ev}$. Those details are the spallation plate (SP) and the layer with the internal mechanically created vapor-liquid mixture (VLM) [10, 11, 14, 15, 16, 19, 20, 22, 23]. The boundary 4'-3 is now the boundary among 4' and the SP. The thicknesses of the SP and VLM is of the order of d_T or d_f if $d_f < d_T$. The SP becomes thinner and thinner as fluence F grow and disappears above the evaporation threshold F_{ev} , here "evaporation" means disappearance of the SP. Thus the internal VLM loses its property to be internal (separated by SP from the tail 4') and above F_{ev} contacts directly with the vapor 4'. Consequently, for $F > F_{ev}$ the boundary 4'-3 separates vapor 4' and vapor-liquid mixture (VLM). This transformation of the right (in Fig. 1a) neighbor 3 of the boundary 4'-3 from the continuous state to the VLM state is clearly seen in the MD simulations in Figs. 14, 15 in [26] and Fig. 16 in [27]. Those simulations were done for a variety of fluences from below of the threshold F_{abl} to above the threshold F_{ev} . The threshold F_{ev} is rather high. If temperature T_3 in the point 3 tends to the critical temperature, then the vapor density 4' at the boundary 4'-3 increases, and the ratio of densities at the density jump 4'-3 decreases. In the dense vapor 4' the condensation process begins.

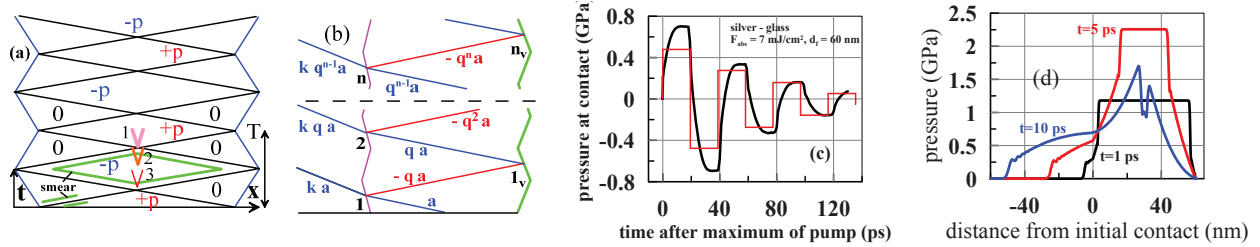


FIGURE 2. (a) Undamped oscillations caused by decay of a two side pressure jump into vacuum. At the instant $t = 0$ (along the x -axis) we have a homogeneous state $p > 0$ ("+"). There are an oscillating sequence of expansions "+" and stretchings "-". They are separated by the triangles "0" where the pressure is equal to the vacuum pressure. There are the sharp jumps from "+" to "0" and to "-" if amplitude p is small (linear approximation, see the end of §3). For the larger amplitudes the jumps smear into transition layers like the layer 2 in Fig. 1(a). This is shown by the lines "smear". If a tensile stress in the middle plane in the first rhombus "-"p" overcomes a material strength then spallation begins. This is shown as the divergent pairs (or angles) 1, 2, or 3. These pairs symbolize the divergence of two halves of a film after spallation. The position of the tip point of the pair on the time axis going along the middle plane is defined by the pressure dependence $p(t) < 0$. In the case of negligible smearing, the dependence $p(t)$ in the first rhombus is a rectangular function. Then at the ablation threshold F_{abl} the separation begins in the point 1 because this point corresponds to the piece of matter under the longest in time stretching. In the case of significant smearing the largest $|-p|$ value is achieved near the central region of the rhombus: this is the case when spallation at the threshold F_{abl} begins in the tip point 2. For the higher fluences $F > F_{abl}$ the tip is gradually shifted to more early instants 2→3. Those instants are closer to the instant when pressure changes its sign. (b) Escape of waves from the resonator (this is the film) when the resonator is in contact with substrate. The quickly heated film begins to expand to the left to substrate and to the right to vacuum. The expansions at the first half periods are alternated with the contractions at the second half periods, see Fig. 2(a). The contact and the vacuum boundary are shown as the lilac and the green zigzag lines, resp. The blue lines are the Π (plus) characteristics $x + c_s t$, while the red lines are the M (minus) characteristics $x - c_s t$. (c) Decaying oscillations of pressure at the contact. They were observed experimentally in [6]. Comparison of solutions, the one obtained by the two-temperature hydrodynamics Lagrangian code and the second from a linear acoustics (the rectangular curve). Duration of pulse is 100 fs, $F_{abs} = 7 \text{ mJ/cm}^2$, silver film, $d_f = 60 \text{ nm}$. We take the maximum pressure $p = 2.25 \text{ GPa}$ from this particular simulation and calculate the linear solution with $a = b = p/2$. Here a and b are values carried along the Π and M characteristics, resp. Plastic speed of sound for Ag is 3.1 km/s, normal density 10.49 g/cc. We take the plastic speed c_s because simulations have been done with a plastic equation of state. Glass is pyrex $c_s = 3.9 \text{ km/s}$, density 2.23 g/cc; $\eta = 0.27$. (d) Evolution caused by action of an ultrashort pulse with parameters presented in Fig. 2(c). Initially glass is $x < 0$, while film occupies $0 < x < 60 \text{ nm}$. As was said in §2, duration t_T of leveling of electron temperature T_e is fast, less than 1 ps. Therefore it is insignificant from what side of the film the film was illuminated. We see that total pressure $p = p_e + p_i$ increases during the two-temperature relaxation because the ion Gruneisen parameter is larger, see §2. There is a shock propagating into glass. The contact seen as a kink on a pressure profiles moves with small (absorbed energy is small) subsonic velocity $\approx 50 \text{ m/s}$.

5. Overexpansion as result of amplification caused by interplay of two rarefaction waves

Figures 1(a,b) illustrate the flow with *one rarefaction* wave unloading a homogeneous half-space. In hydrodynamics of gas this flow is called the decay of a pressure jump into vacuum. In this case a substance expands exactly to such an extent that the dynamical boundary condition with the external medium is fulfilled. It is remarkable that this occurring once stretching is impossible in case of a film surrounded by vacuum from the two sides, in this case the overstretching is necessary. Figures 1(c,d) show the changes caused by the spatial inhomogeneity connected with a heating depth d_T in the case of a bulk target. The inhomogeneity introduces the scale and thus breaks the self-similarity. In the simplest inhomogeneous case, we have a freestanding, instantaneously heated film [15, 19]; the inhomogeneity appears thanks to the second free boundary; the scale breaking the self-similarity is the thickness d_f of a film. Then *two rarefaction* waves starts to propagate towards each other from the two vacuum boundaries as it is shown in Fig. 2(a). They intersect in the central plane, after that the negative pressures are created, and the layer under a tensile stress begins to expand outside from the central plane. Later the rarefaction waves reflect from the opposite boundaries, and again intersect in the center returning positive pressure, and continue those oscillations stretching and compressing a film. Thus we obviously see that the single rarefaction wave can exactly adjust its expansion degree to the boundary demand but that the two of them cannot - overexpansions and oscillations appear.

Amplitude of oscillations increases as energy F_{abs} rises. Above the ablation threshold F_{abl} the film is teared to two pieces as it is shown by divergent pairs 1, 2, or 3 in Fig. 2(a). The divergent lines in the angles 1-3 symbolize the divergence of the two new coasts of the disrupted condensed medium. Velocity of divergence is small relative to sound

speed. Acoustic characteristics running ahead the lines 1-3 decrease pressure to the vacuum value. In the zone covered by those characteristics the flow totally changes in comparison to the flow without spallation disruption. Distance between the disrupted halves increases. Thickness of the gaps 1-3 oscillates but an average thickness gradually grows in time. A phase of oscillations and its period change relative to the oscillations of a whole film. Near threshold F_{abl} the period of oscillations of the halves is twice less than the period T of a whole film. The period T is marked by the two-side arrow "T" in the right corner of Fig. 2(a).

Dynamics of a quickly heated film qualitatively alters in the case when a film contacts with a substrate relative to the case of the freestanding film, see Fig. 2(b). Quantitatively those changes are small during the period "T" of the first oscillations if the ratio $\eta = z_{subs}/z_{film}$ is small; here z_{film} , z_{subs} are acoustic impedances of a film and a substrate, resp. The ratio η is small when a dense rigid film is placed against a weak substrate as in the case of a gold or silver film on a glass support. This is the flow presented in Fig. 3 in [18] where a spatiotemporal acoustic diagram of the waves running the film is shown for the case when a film delaminates from a substrate. Here in Fig. 2(a) we show, firstly, a picture of acoustic oscillations in a form of a standing wave and, secondly, we present description of an interplay of the delamination process and the internal spallation of a film. Those standing wave and interplay were not considered in [18]. Spatial wavelength λ of the standing wave is $\lambda = 2d_f$. Thus this is the lowest mode admitted by the boundary conditions.

Oscillations of a film in contact with a substrate decay in time as a result of radiation of acoustic waves into substrate, see Fig. 2(b). Let us describe this in the linear approximation $|p| \ll K$, $|u| \ll c$. We suppose that the oscillations are adiabatic and that an initial distribution of pressure is homogeneous. There are propagating to the left side and propagating to the right side families of characteristics $\{p = \Pi a, u = -\Pi a/z\}$ and $\{p = Mb, u = Mb/z\}$, here p, u are perturbations of pressure and velocity; $\Pi(x + c_s t)$ is a function defining the "plus" (Π) characteristics running from right to left (shown in blue in Fig. 2b), $\Pi(x) \equiv 1$, $x \in [0, d_f]$, $x = 0$ is initial position of a contact; $M(x - c_s t)$ is a function defining the "minus" (M) characteristics running from left to right (shown in red in Fig. 2b), $M(x) \equiv 1$, $x \in [0, d_f]$; a, b are values carried along the "plus" and "minus" characteristics, resp.; z is an acoustic impedance. The Π characteristics starting inside the film $x \in [0, d_f]$ reflects and transmits the metal-glass contact in the point 1 shown in Fig. 2(b). In the linear approximation, the transmitted and reflected amplitudes are proportional to the amplitude a . The coefficients of reflection ($-q$) and transmission k are defined from the conditions of continuity of pressure and velocity across the contact: $ka = a - qa$, $-ka/z_{subs} = -a/z_{film} - qa/z_{film}$. Thus the coefficients are $q = (1 - \eta)/(1 + \eta)$ and $k = 2\eta/(1 + \eta)$, where $\eta = z_{subs}/z_{film}$. The "minus" (M) characteristics in the substrate carry value $a = 0$, and the "plus" ($x + c_s t$) characteristics Π in the substrate carry the transmitted value ka . The sum of the values carried by M and Π characteristics defines the left sides of the continuity conditions for pressure and velocity in a substrate. The same should be said about the right (film) side of those conditions.

The characteristics a shown in Fig. 2(b) after reflection from the point 1 becomes the M characteristics $-qa$. The M characteristics $-qa$ reflects from the vacuum (v) boundary in the point 1_v and after that it changes sign $-qa \rightarrow qa$ and converts to the Π type. It again reflects back and transmits into the substrate in the point 2 at the contact. The amplitude incoming into the point 2 is qa , see Fig. 2(b). We easily obtain the second generation of waves using the same coefficients of reflection ($-q$) and transmission k as were used above for the point 1 but now for the point 2. In this way we come to the geometrical progression shown in Fig. 2(b). This progression gives a positive pressures in the half periods of the train of periods irradiated into substrate from the oscillating film.

The negative part of the train is formed by the flux of the M characteristics running to the right side from the axis $t = 0$ to the vacuum boundary providing its expansion into vacuum during the first half period, see Fig. 2(b). This homogeneous flux carries a value a . After reflection from the vacuum boundary, the M type converts to the Π type and the transported value changes its sign: $a \rightarrow -a$. Thus the Π characteristics carrying the value ($-a$) propagates from the vacuum side to the contact. This Π characteristics arrives to the second knee (the second half period) of the zigzag contact line where the contraction of a film takes place in Fig. 2(b). It is interesting that the coefficients of reflection ($-q$) and transmission k again remains the same as in the point 1. Another geometrical progression is formed by successive repeating of the reflections and transmissions.

The value a equals to $a = p/2$ for the fast heating, where p is homogeneous pressure marked as "+p" in Fig. 2(a). Every period $T = d_f/c_s$ (shown in Fig. 2a) of the irradiated wave consists from the positive and negative half periods. Absolute values of pressures are equal at those half periods. The rectangular train is $\pm k(p/2)\Pi$, $\pm kq(p/2)\Pi$, $\pm kq^2(p/2)\Pi$, ..., where $\Pi(x + c_s t)$. Instant spatial profile is given by $\Pi(x + c_s t_{fix})$, and the pressure alternating at the contact shown in Fig. 2(c) is $\Pi[(x = 0) + c_s t]$. Fig. 2(d) demonstrates how the pressure profiles evolve during the first quarter of the period $T \approx 40$ ps defined in Fig. 2(a) and given in Fig. 2(c). In the hydrodynamic simulation [21, 28] shown in Fig. 2(c,d) the two-temperature equation of state from [28], two-temperature heat conductivity from [29],

and coupling parameter [29] were used. The analytical linear solution with a substrate tends to the solution for the freestanding film when the impedance ratio is small $\eta \ll 1$ (soft substrate). Then pressure in the first left triangular (see Fig. 2a) is small $p\eta/(1+\eta)$. It is positive because a substrate resists to expansion. Amplitude of oscillations shown in Fig. 2(c) decays e-times after $1 + 1/(2\eta) \approx 3$ and 4.4 periods for Ag/glass and Au/glass pairs, resp.

6. Delamination or internal spallation - the choice is dictated by strength of adhesion to glass

From Fig. 2 it is clear that the fast ($\tau_L < t_T$) heating of a metal film produces tensile stresses ($p < 0$) acting in a film and in a substrate. It is important that the stress amplitudes operating at a contact are significantly $\approx 1/\eta$ -times less (≈ 4 for Ag/glass, ≈ 7 for Au/glass) than in the central layer of a film. The adhesion strength p_{adh} between glass and film depends on many parameters such as the details of coating, state of a surface before coating, or on addition of a thin interlayer. E.g., it is known that for the pure Ag/glass and Au/glass pairs the adhesion p_{adh} is small, while addition of the chromium interlayer between Au and glass strongly increases p_{adh} . In case when $p_{adh} = 0$, the film delaminates as a whole from the substrate when the first characteristics of the flux (once reflected from the vacuum boundary at the right side of Fig. 2a,b) arrives at the contact. This is the instant $t_s = d_f/c_s + 0$ when the zigzag contact line does its first kink from compression to dilution. If $p_{adh} = 0$ then the delamination threshold is $F_{delam} = 0$. The threshold F_{delam} increases as the strength p_{adh} grows. If p_{adh} is smaller than the material strength of a glass then the spallation in glass is impossible - a film delaminates before than glass may be damaged. Delamination phenomenon is used in applications [1, 2, 3, 4, 5] and was considered in [5, 18].

If a tensile stress in a film overcomes the material strength of metal then the spallation inside a film begins, see the angles 1, 2, and 3 in Fig. 2(a). Corresponding threshold is an ablation threshold $F_{abl} + \Delta F$. We have $0 < F_{delam} < F_{abl} + \Delta F$ for small values of adhesion p_{adh} . Increasing of p_{adh} increases F_{delam} up to a value $F_{abl} + \Delta F$. This is possible because the value p_{adh}^* corresponding to $F_{delam} \approx F_{abl}$ is $1/\eta = 4-7$ times smaller than the internal tensile stresses acting in the Ag or Au films; thus to close the delamination, it is not necessary to have a very high values of adhesion p_{adh} higher than a material strength of the strong continuous metals. A film delaminates as a whole (without internal spallation) in the range of fluences $F_{delam} < F < F_{abl} + \Delta F$. It is said "to close the delamination". Indeed, below it is shown that for the larger fluences $F > F_{abl} + C * \Delta F$ the hydrodynamic delamination as a result of interplay of waves at the acoustic stage of a film-substrate interaction becomes impossible, here $C \geq 1$. The delamination means that a contact becomes broken and a gap between metal and glass appears and grows. The positive addition ΔF is small $\Delta F \rightarrow 0$ if the ratio is small $\eta \rightarrow 0$. The value F_{abl} here is an ablation threshold for a freestanding film ($\eta = 0$).

7. Decay of a film into two halves and deceleration of the internal half by the substrate

Spallation of a film into two halves takes place above an ablation threshold $F > F_{abl} + \Delta F$. For the weak substrate $\eta \ll 1$ those halves are approximately symmetric to each other. Spallation results from inertia and limitation on material strength. During the stage when a pressure along the vertical line $x = d_f/2$ in Fig. 2(a) is positive the two halves (h) accumulate momentum $\mu_h(t) = \int_0^t p(x = d_f/2, t') dt'$ of the opposite signs per unit of a film surface. Corresponding average or centrum of mass velocities of the halves are $v_h = \mu_h(t)/(\rho d_f/2)$, where ρ is initial density of a metal. The pressure is positive in the lowest triangular "+p" in Fig. 2(a). After acceleration of the halves into the opposite sides in the triangular "+p" (velocity $|v_h|$ increases, $p > 0$), the deceleration begins (decreasing $|v_h|$, $p < 0$); because condensed matter resists ($p < 0$) to stretching. The deceleration takes place in the rhombus "-p" in Fig. 2(a).

Slightly above an ablation threshold, in our conditions with inhomogeneous pressure profiles shown in Fig. 2(d), the spallation starts in the region near the center of the rhombus "-p" in Fig. 2(a), the angle 2. At the ablation threshold the velocity $|v_h(t)|$ drops down to zero $v_h^{spall} = v_h(t = t_{tip}) = 0$ in the tip $t = t_{tip}$ of the angle 2 in Fig. 2(a). The substrate affects the deceleration process changing the reflected flux of Π characteristics, see Fig. 2(a,b). This action does weaker the left rarefaction wave, thus increasing the threshold $F_{abl} \rightarrow F_{abl} + \Delta F$ in comparison with a freestanding film. Accumulation of momentum $\mu_f(t) = \int_0^t p_{cb}(t') dt'$ and a centrum of mass velocity $v_f = \mu_f/(\rho d_f)$ of a whole film (f) takes place at the contact boundary (cb). Condition $v_f \sim v_h$ defines the shift up ΔF of the threshold F_{abl} . Velocity v_h increases fast with an increase of fluence above the threshold, while velocity v_f increases slowly if the ratio of impedances η is small, because $\langle p_{cb} \rangle \sim \eta \langle p(x = d_f/2, t) \rangle$. Therefore in the vicinity of ΔF above the threshold $F_{abl} + \Delta F$ the internal half of a film (the left half "lh" in Fig. 2a,b) has a centrum of mass velocity v_{lh}^{spall} directed to the substrate.

It is important that the left half flying to the left side cannot recoil and change velocity to the positive direction as a result of deceleration by substrate, thus remaining in contact with a substrate (no delamination). To show this we

use the solution with multiple reflections/transmissions from §5 presented in Fig. 2(b). The Π characteristics starting from the axis $t = 0$ carry a value a , while the M ones carry b . In the case considered in §5 we have $a = p_0/2$, $b = a$, where p_0 is pressure inside the triangular ”+p” in Fig. 2(a). Then the alternating of signs of pressure at a contact takes place. Now we have to change the carried values to $a = |v_{lh}^{spall}|z/2$, $b = -a$. Then we see that the contact pressure is always positive and exponentially monotonically decays: during the first period ”T” $p_1 = (\eta/(1 + \eta))z|v_{lh}^{spall}|$, see Fig. 2(a) for definition of a period; the second period $p_2 = qp_1$; ...; the n -th period $p_n = q^{n-1}p_1$, where a reflection coefficient is $q = (1 - \eta)/(1 + \eta)$ as in §5. Pressure decays e-times after the $1 + 1/(2\eta)$ periods. Simulations with the full two-temperature hydrodynamic Lagrangian code supports this picture of impinging. Summing the shifts $u_n T$ after the infinite number of periods we find a final position of a contact. Its position is $(v_{lh}^{spall}/c_s)d_f$ to the left side relative an initial position $x = 0$.

In conclusion it should be emphasized that the presented study of dynamics of a film on support is significant for applications where a wide variety of configurations of well or pure attached films of different thickness are used. The study provides a base for understanding how the diversified nanostructures on the film coated targets are formed. It explains why in one case the open glass remains in the irradiated spot (low fluence, weak adhesion) while in the other cases there are remnants of film on a substrate and a crater like structure is formed (higher fluence or/and strong adhesion).

Authors acknowledge support from Russian Science Foundation 14-19-01599.

REFERENCES

- [1] U. Zywiets, A. B. Evlyukhin, C. Reinhardt, and B. N. Chichkov, *Nature Communications* **5**, 3402 (2014).
- [2] A. Kuchmizhak, A. Ionin, S. Kudryashov, S. Makarov et al., *Optics Letters* **40**, 1687–1690 (2015).
- [3] Y. Nakata, T. Okada, and M. Maeda, *Jpn. J. Appl. Phys.* **42**, L1452 (2003).
- [4] Y. Nakata, K. Tsuchida, N. Miyanaga et al., *JLMN-Journ.of Laser Micro/Nanoengin.* **3**, No. 2, 63–66 (2008).
- [5] C.M. Rouleau, C.-Y. Shih, C. Wu, L.V. Zhigilei, A.A. Puretzky et al., *Appl. Phys. Lett.* **104**, 193106 (2014).
- [6] J. Wang and Ch. Guo, *Appl. Phys. A* **111**, 273–277 (2013).
- [7] P. Fons, P. Rodenbach, K.V. Mitrofanov et al., *Phys. Rev. B* **90**, 094305 (2014).
- [8] N.A. Inogamov et al., *Appl. Surf. Sci.* **255**, No. 24, 9712–9716 (2009); arXiv:0812.2965 [physics.optics].
- [9] N.A. Inogamov, V.V. Zhakhovskii, S.I. Ashitkov et al., *Contrib. Plasma Phys.* **51**, No. 4, 367–374 (2011).
- [10] D.S. Ivanov and L.V. Zhigilei, *Phys. Rev. B* **68**, 064114 (2003).
- [11] L.V. Zhigilei, Z. Lin, and D.S. Ivanov, *J. Phys. Chem. C* **113**, 11892 (2009).
- [12] K. Sokolowski-Tinten, J. Bialkowski, A. Cavalleri et al., *Phys. Rev. Lett.* **81**, 224–228 (1998).
- [13] N.A. Inogamov, S.I. Anisimov, B. Retfeld, *JETP* **88**, No. 6, 1143–1150 (1999).
- [14] S.I. Anisimov, N.A. Inogamov, A.M. Oparin, B. Retfeld et al., *Appl. Phys. A* **69**, No. 6, 617–620 (1999).
- [15] S.I. Anisimov, V.V. Zhakhovskii, N.A. Inogamov, K. Nishihara et al., *JETP Lett.* **77**, No. 11, 606–610 (2003).
- [16] B. Chimier and V.T. Tikhonchuk, *Phys. Rev. B* **79**, 184107 (2009).
- [17] B. Chimier, *EuroPhys. Lett.* **92**, 15001 (2010).
- [18] N.A. Inogamov and V.V. Zhakhovskii, *JETP Lett.* **100**, No. 1, 4–10 (2014).
- [19] A.K. Upadhyay, N.A. Inogamov, B. Retfeld, H.M. Urbassek, *Phys. Rev. B* **78**, 045437 (2008). [10 pages].
- [20] S.I. Anisimov, N.A. Inogamov, Yu.V. Petrov, V.A. Khokhlov et al., *Appl. Phys. A* **92**, No. 4, 939–943 (2008).
- [21] N.A. Inogamov, V.V. Zhakhovskii, Yu.V. Petrov et al., *Contrib. Plasma Phys.* **53**, No. 10, 796–810 (2013).
- [22] M.E. Povarnitsyn, T.E. Itina, M. Sentis, K.V. Khishchenko et al., *Phys. Rev. B* **75**, 235414 (2007).
- [23] M.E. Povarnitsyn, K.V. Khishchenko, and P.R. Levashov, *Appl. Surf. Sci.* **255**, 5120–5124 (2009).
- [24] M.E. Povarnitsyn, P.R. Levashov, and K.V. Khishchenko, arXiv: 1411.2241 [physics.comp-ph].
- [25] A.V. Mazhukin, V.I. Mazhukin, M.M. Demin, *Appl. Surf. Sci.* **257**, 5443–5446 (2011).
- [26] N.A. Inogamov, V.V. Zhakhovskii, S.I. Ashitkov, Yu.V. Petrov, M.B. Agranat et al., *JETP* **107**, 1–19 (2008).
- [27] Ch. Wu, L.V. Zhigilei, *Appl. Phys. A* **114**, 11–32 (2014).
- [28] Yu.V. Petrov, K.P. Migdal, N.A. Inogamov, V.V. Zhakhovskii, *Appl. Phys. B* **119**, 401–411 (2015).
- [29] Yu.V. Petrov, N.A. Inogamov, and K.P. Migdal, *JETP Lett.* **97**, No. 1, 20–27 (2013).